Supporting Information for

Fluorophore Branching Boosted Photo-induced Energy Transfer in UiO-66 for Ultrasensitive and Instant Hydrazine

Ying Luo,[ab] Da Lei,[*b] Maohua Li,[c] Yuansheng Ge,[b] Jiguang Li,[b] Baiyi Zu,[bc] Jun Yao,[*a] and Xincun Dou[*bcd]

[a.] School of Pharmacy, Xinjiang Medical University, Urumqi, 830000, China. E-mail: xydyaojun2022@xjmu.edu.cn

[b.] Xinjiang Key Laboratory of Trace Chemical Substances Sensing, Xinjiang Technical Institute of Physics and Chemistry, Chinese Academy of Sciences, Urumqi 830011, China. E-mail: leida@ms.xjb.ac.cn; xcdou@ms.xjb.ac.cn

[c.] Key Laboratory of Improvised Explosive Chemicals for State Market Regulation, Urumqi 830011, China.

[d.] Center of Materials Science and Optoelectronics Engineering, University of Chinese Academy of Sciences, Beijing 100049, China.

* Corresponding authors. E-mail: xydyaojun2022@xjmu.edu.cn (Jun Yao); leida@ms.xjb.ac.cn (Da Lei); xcdou@ms.xjb.ac.cn (Xincun Dou)

1. Preparation of the test solutions and the testing process

1.1. Preparation of UiO-66-Flu suspension liquid (0.5 mg/mL)

250 mg of UiO-66-Flu powder was dissolved in 500 mL of DMF, and the evenly mixed UiO-66-Flu suspension liquid was obtained after 10 min of ultrasonication.

1.2. Preparation of the hydrazine stock solution

10 mmol of hydrazine was dissolved in deionized water to prepare a hydrazine stock solution at a concentration of 10 mM, which was then diluted with deionized water to obtain hydrazine solutions of various concentrations.

1.3. Optimization of the hydrazine detection system

Effect of solvents: 5 mg of the UiO-66-Flu was dissolving into 10 mL of methanol, ethanol, dimethyl sulfoxide (DMSO), dichloromethane (CH_2Cl_2), and N, N-dimethylformamide (DMF) solvent, respectively, and then 1 mL of hydrazine solution (10 mM) was added, the fluorescence intensity of the UiO-66-Flu was examined before and after adding hydrazine solution, respectively. As shown in Fig. S15, the result illustrates that the optimal solvent environment determined by the change of the fluorescence intensity at 528 nm before and after adding hydrazine solution was DMF. Finally, DMF ethanol was chosen as the optimized solvent for the sensitive monitoring of hydrazine.

Effect of the UiO-66-Flu concentration: As illustrated in Fig. S16, when the concentration of UiO-66-Flu in DMF was fixed at 0.5 mM, the greatest change of the fluorescence intensity at 528 nm after adding hydrazine solution (10 mM) was observed. Therefore, 0.5 mg/mL of UiO-66-Flu was selected as the optimized concentration for the sensitive monitoring of hydrazine.

1.4. Testing of hydrazine solution

Spectral response testing of the UiO-66-Flu: 1 mL of hydrazine solution of different concentrations (125, 200, 250, 300, 400, 500, 600, 750 and 1000 μM) was added to 1 mL of UiO-66-Flu solution (0.5 mg/mL) in a cuvette, respectively. The obtained mixture solution was used for the direct measurement of the fluorescence spectra (λ_{ex} = 290 nm; Slits: 0.5 nm; λ_{em} = 528 nm; Slits: 5.5 nm; Spectrometer: Edinburgh FLS1000). The time-dependent spectral characteristics were measured and recorded with the portable fluorescence sensing platform (Maya 2000 pro).

1.5. Preparation and detection of trace analytes

Analyte stocks solution: Acrylamide, Urea, Thiourea, $NiCl_2$, $BaCl_2$, $CuCl_2 \cdot 2H_2O$, $CaCl_2$, $CuSO_4$, NaH_3PO_4, L-Tyrosine, L-Isoleucine, L-Valine, L-Cysteine, Glycine, H_3BO_3, $C_2H_2O_4$, $C_{12}H_{25}NaO_3S$, $C_{12}H_{25}NaO_4S$, D-Glucose, $C_6H_{12}O_6$, and $C_{12}H_{22}O_{11}$ were dissolved in DMF to the prepare analyte stock solutions at concentrations of 1 and 2 mM, respectively.

Selective detection process: Stock solutions (4 mM, 1 mL) of certain analytes were added into a cuvette containing 1 mL of UiO-66-Flu suspension liquid. After the reaction, the fluorescence spectra and images were measured and recorded (λ_{ex} = 290 nm, slit: 0.5 nm, λ_{em} = 528 nm, slit: 5.5 nm, Spectrometer: Edinburgh FLS 1000).

Anti-interference test process: A mixture of stock solutions (4 mM, 0.5 mL) and nitrite stock solutions (4 mM, 0.5 mL) for certain analyte were added into a cuvette containing 1 mL UiO-66-Flu suspension liquid. After the reaction, the fluorescence spectra and images were measured and recorded (λ_{ex} = 290 nm, slit: 0.5 nm, λ_{em} = 528 nm, slit: 5.5 nm, Spectrometer: Edinburgh FLS 1000).

1.6. UiO-66-Flu sensor reusability test

Preparation of UiO-66-Flu suspension liquid: Dissolve 5 mg of UiO-66-Flu powder in 1 mL of DMF and sonicate for 10 min to obtain a well-mixed UiO-66-Flu suspension.

Reusability test: Hydrazine solution (1 mM, 1 mL) was added to the above prepared UiO-66-Flu suspension, and the fluorescence spectrum was measured in a cuvette (λ_{ex} = 290 nm; slits: 0.5 nm; λ_{em} = 528 nm; slits: 5.5 nm; Spectrometer: Edinburgh (FLS1000). After three washes by centrifugation with DMF, 1 mL of DMF was added and sonicated for 10 min. Hydrazine solution (1 mM, 1 mL) was added to this suspension, and the above experimental steps were repeated four times.

2. Preparation and testing of the UiO-66-Flu loaded PVDF film (UiO-66-Flu/PVDF) for gaseous hydrazine detection

2.1. Preparation of Pure PVDF film

The first step was to manufacture the pure polymer membrane for the purpose of comparison with those containing increased amounts of UiO-66-Flu. To prepare the pure polymer membrane, PVDF (0.15 g) was dissolved in DMF (1.9 mL) and stirred for 24 h, resulting in a sticky solution.

2.2. Preparation of the UiO-66-Flu/PVDF film

UiO-66-Flu (9.5 mg) was added into the above pure polymer solution to form a homogeneous solution by stirring for 24 h. Before the membrane casting, three intervals of sonication for 15 min were implemented to ensure a very good dispersive solution. Then, the polymer solution in the array slot was scraped flatly with a slide and dried to form a film at about 25 ℃ to obtain a sensing chip for gaseous hydrazine sensing test.

2.3. Sensing test of the sensing unit for gaseous hydrazine

The sensing chips were placed in gaseous hydrazine and tested for 0 s, 0.5 s, 1 s, 2 s, 4 s, respectively. At the same time, the optical images under 365 nm light excitation were recorded with the smartphone.

2.4. Gaseous hydrazine test

Saturated gaseous hydrazine was obtained by placing 0.1 mL of 85% hydrazine into a 500 mL sealed flask and heating to 130 ℃. Certain amount of saturated gaseous hydrazine was injected into a 250 mL sealed flask using a syringe to obtain a reserve gas at a concentration of 343 ppb. The UiO-66-Flu/PVDF films were separately placed in 20 mL sealed flasks, and different volumes of the above reserve gaseous hydrazine (34, 51, 69, 86, 120, 137, 154, and 171 ppb) were injected

3

into the flasks. After 30 s, the fluorescence images of the UiO-66-Flu/PVDF film were recorded with a camera under a 365 nm UV lamp.

3. Calculation Details

All geometric structure optimization tasks of the computational models for the MOF clusters were calculated by the Gaussian 09[1] program using PBE0 exchange-correlation functional with Grimme's DFT-D3(BJ) empirical dispersion correction abbreviated as PBE0-D3(BJ) with def2-SVP[2]. The hybrid functional PBE0 used in the calculation has been proved to be suitable for the modeling of the ground state and excited state properties of the transition metal material and is qualitatively consistent with the experimental study.[3-7] To investigate the solvent effect, the polarizable continuum model (PCM)[8] was employed to simulate the N,N-dimethylformamide DMF environment. A larger basis set def2-TZVPP[2, 9] was adopted to obtain higher quality wave functions.

The transition state searching analysis was performed at the CAM-B3LYP/def2-SVP level and the transition state species were ensured to have only one virtual frequency. Intrinsic reaction coordinate (IRC) calculations were also performed to ensure one transition state connect with two appropriate local minima in the reaction paths. The Gibbs free energies (E_{Gibbs}) at 298.15 K was obtained in Shermo software[10] according to $E_{Gibbs} = E_{elec} + E_{corr}$, and the frequency correction factor of the Zero-point correction (ZPE) was set to be 0.9520[11]. Further, the corresponding structure of the transition state was selected, and combined with the independent gradient model (IGM) analysis [12] to assess weak intermolecular interactions.

In order to simulate the absorption condition, the time dependent density functional theory (TD-DFT) calculations were carried out to obtain the vertical excitation energies for 40 lowest singlet transitions at the PBE0/def2-TZVP level. The emissive properties were estimated based on the optical activity of the lowest singlet transition, in accordance with Kasha's rule[13, 14]. It is well known that the phonon-mediated interband carrier relaxation from the initially excited state to the band edge states, including ligand-/defect-associated states, happening at the picosecond range in MOFs and are much faster than the emission (nanosecond range).[15] Besides, it is reasonable to assume that the emission takes place from the lowest state if it is optically active (large oscillator strength), because such radiative electron-hole recombination is much faster than the nonradiative recombination *via* the intraband multiphonon processes.[16] The convolution of the spectrum was obtained using a gaussian function with a full width at half maximum (FWHM) of 0.3 eV.

All wavefunction analysis was finished by Multiwfn[17] and all isosurface maps were rendered by VMD program[18] based on the outputs of Multiwfn.

Supplementary Figures
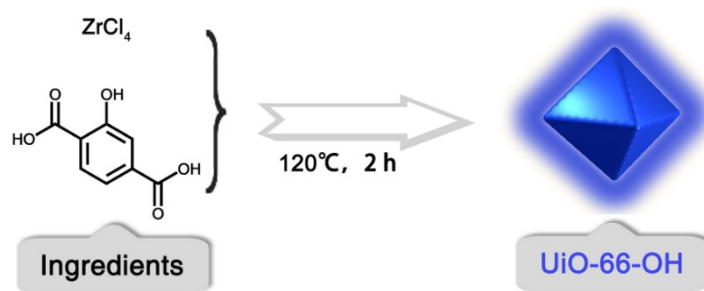
Fig. S1. UiO-66-OH synthesis scheme.
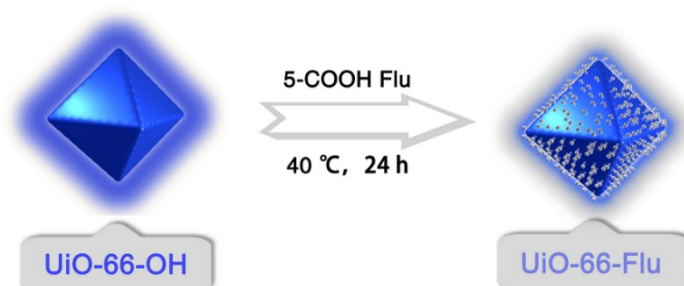
Fig. S2. UiO-66-Flu synthesis scheme.
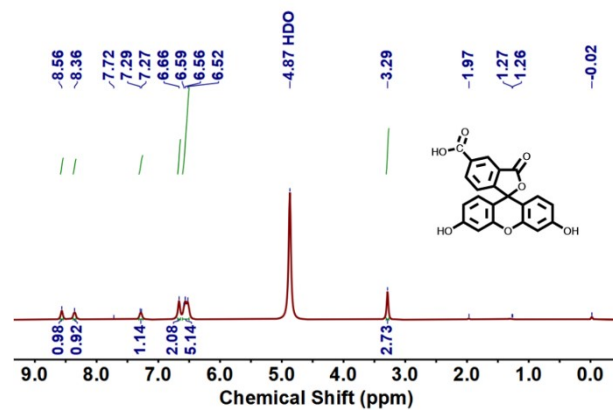
Fig. S3. ^{1}H NMR spectrum of Flu (MeOD, 400 MHz).
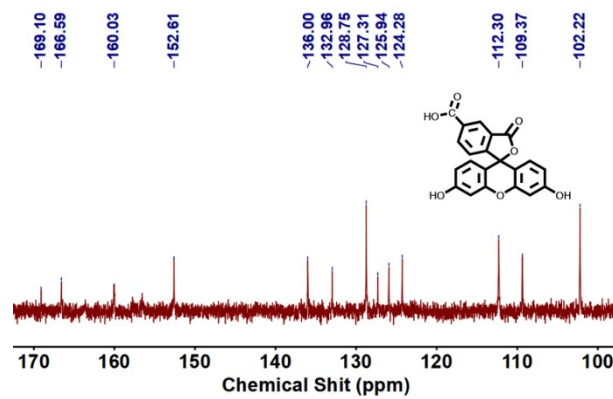
Fig. S4. ^{13}C NMR spectrum of Flu (MeOD,101 MHz).

6
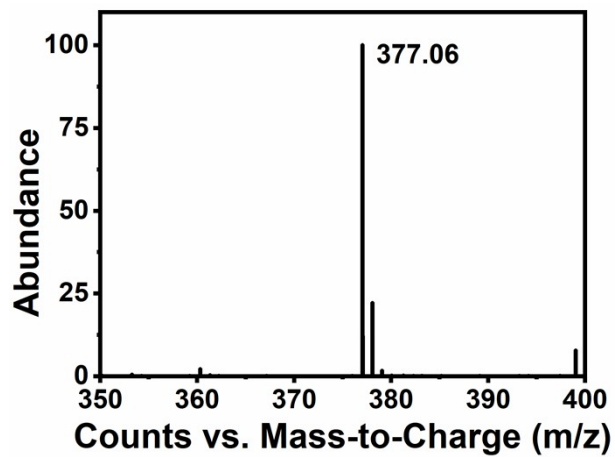
Fig. S5. HRMS spectrum of Flu.
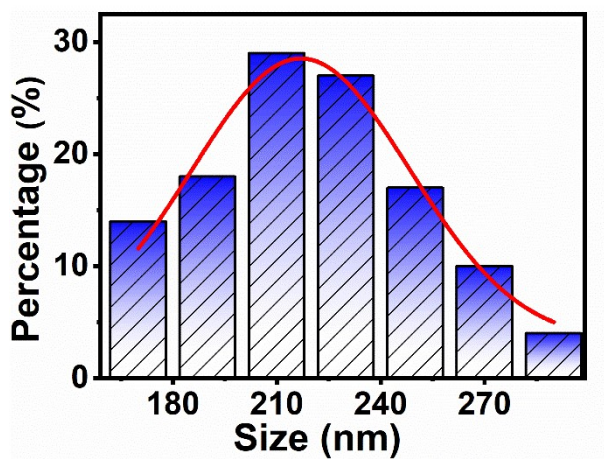
Fig. S6. Statistical analysis of the UiO-66-OH particle size in SEM images (n = 125).
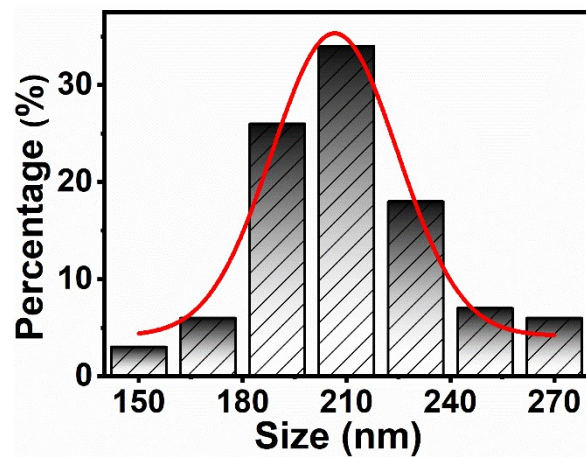
Fig. S7. Statistical analysis of the UiO-66- Flu particle size in SEM images (n = 100).
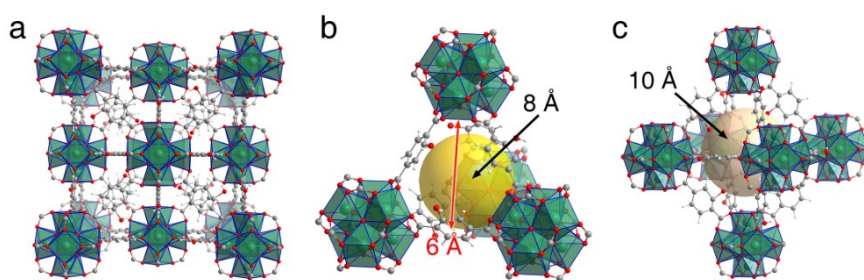
Fig. S8. (a) The entire UiO-66-OH topology, (b) tetrahedral topology, and (c) octahedral topology.
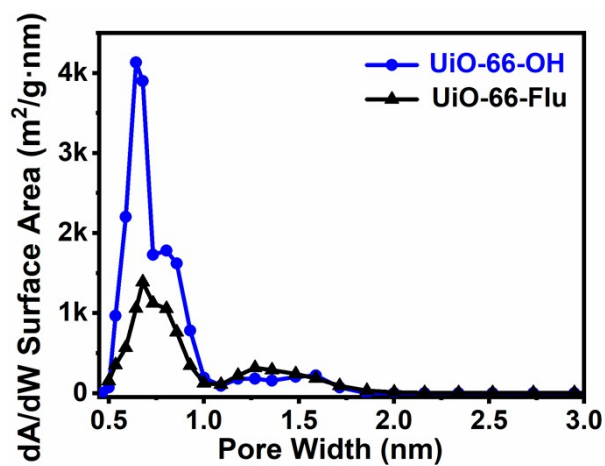
Fig. S9. Pore size distribution of UiO-66-OH and UiO-66-Flu.
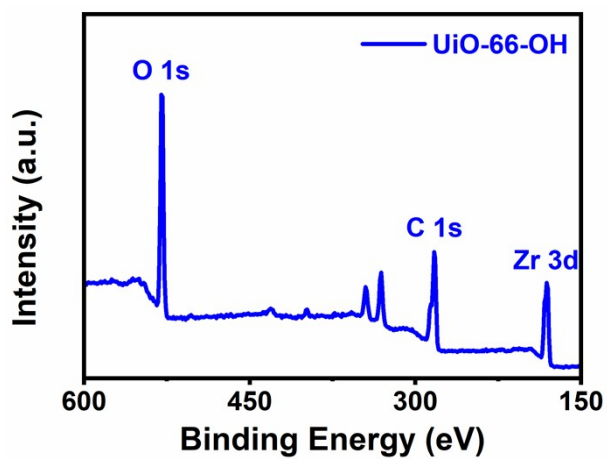
Fig. S10. XPS broad survey spectrum of UiO-66-OH.
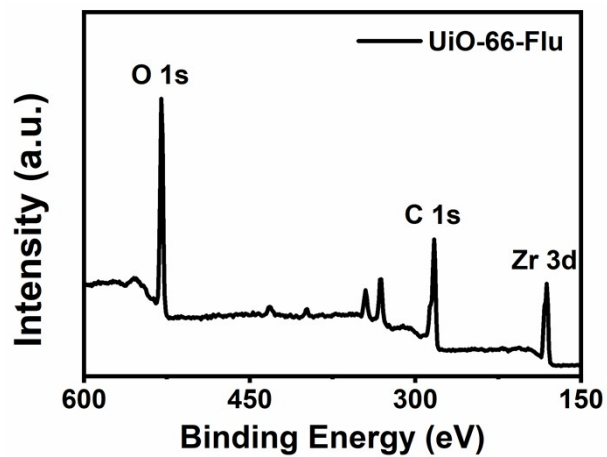
Fig. S11. XPS broad survey spectrum of UiO-66-Flu.
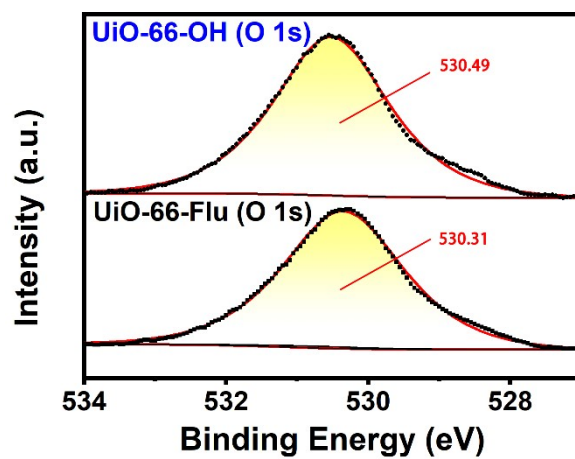
Fig. S12. XPS spectra of oxygen in UiO-66-OH and UiO-66-Flu.
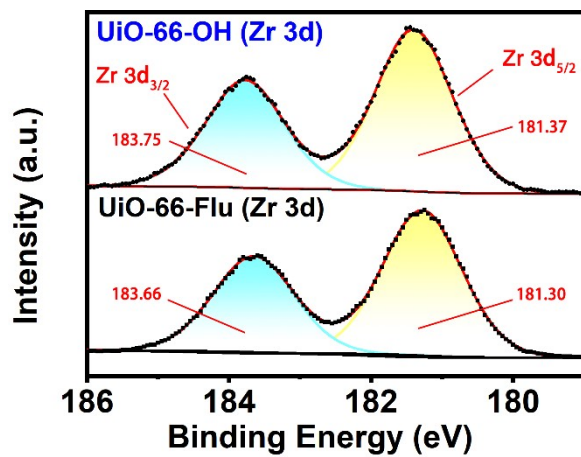
Fig. S13. XPS spectra of zirconium in UiO-66-OH and UiO-66-Flu.
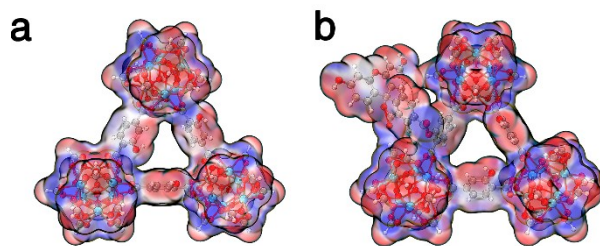
Fig. S14. Electron cloud distribution of (a) UiO-66-OH and (b)UiO-66-Flu.
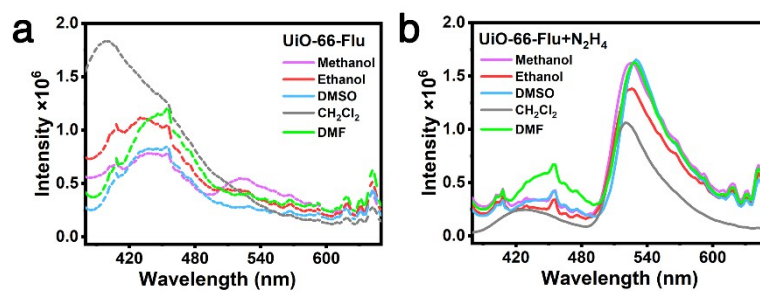
Fig. S15. Solvent effect test: Fluorescence spectrum of (a) UiO-66-Flu suspension liquid before and (b) after adding hydrazine to analyte.
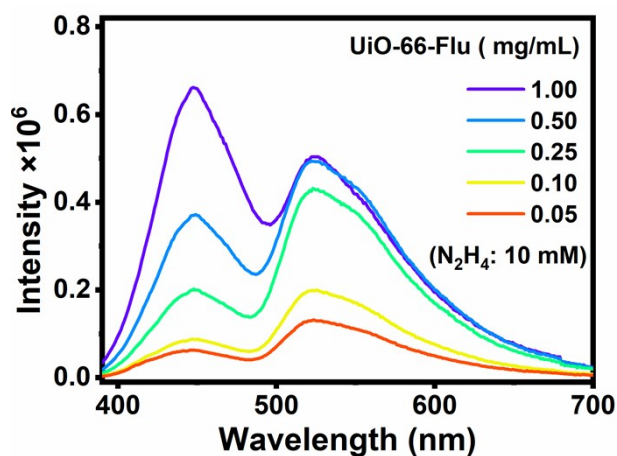
Fig. S16. Fluorescence response of different concentrations of UiO-66-Flu fluorescent suspension liquid against solution hydrazine (10 mM).
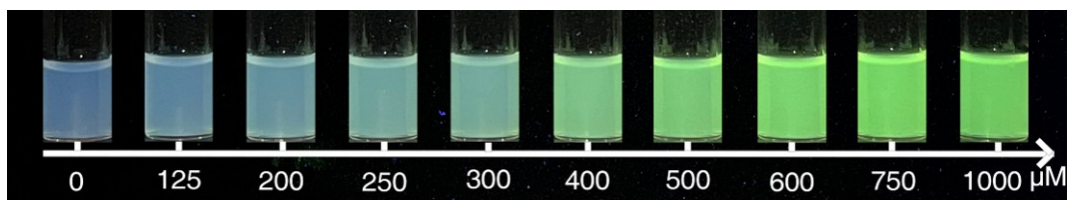
Fig. S17. Photograph of the fluorescence response of the 0.5 mg/mL UiO-66-Flu fluorescent suspension liquid against different concentrations of hydrazine solutions.
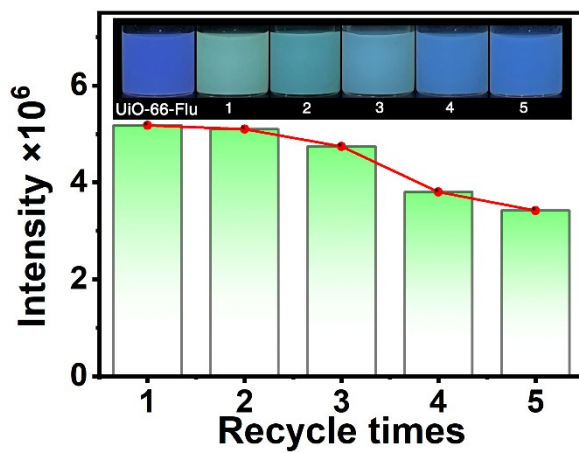
Fig. S18. UiO-66-Flu and its recyclable test results. (Inset: Corresponding fluorescence image)
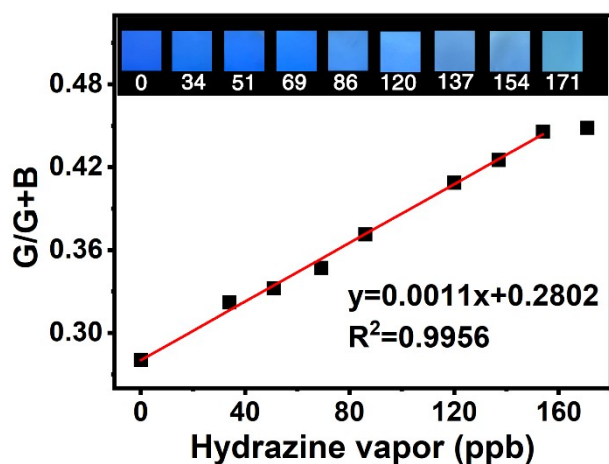
Fig. S19. Plotting curve of G/(G+B) values extracted from the fluorescent images of the UiO-66-Flu/PVDF film toward the gaseous hydrazine samples with various concentrations. (Inset: the corresponding fluorescence images of the UiO-66-Flu/PVDF film.
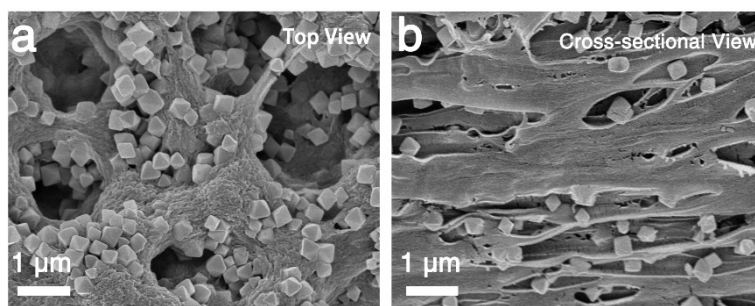
Fig. S20. Corresponding SEM images of UiO-66-Flu/ PVDF film after detection of gaseous hydrazine (a) top view and (b) cross-sectional view.

Fig. S21. Actual application scene.

Table S1. Research progresses in fluorescence detection of hydrazine.

No.	Sensor platforms	Response time (s)	Detection mode	LOD (nM)	Ref.
1		/	Turn on	45	[19]
2		/	Turn on	47	[20]
3		/	Turn on	88	[21]
4		/	Turn on	135	[22]
5		300	Ratiometric	36	[23]
6	**CPDs@ Fe**	/	Turn on	168	[24]
7		/	Turn on	260	[25]
8		180	Ratiometric	58	[26]
9		/	Turn on	36400	[27]
10		/	Turn on	196	[28]
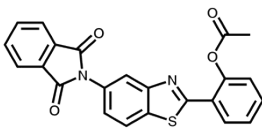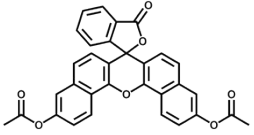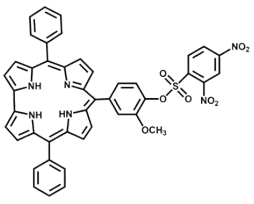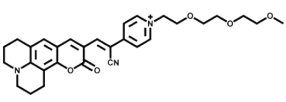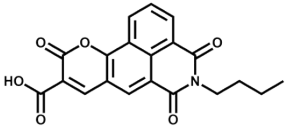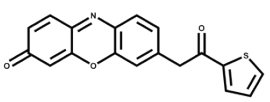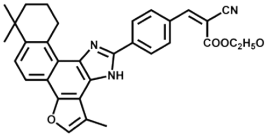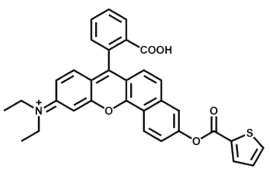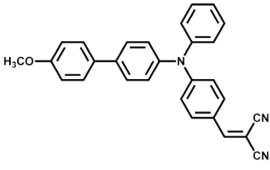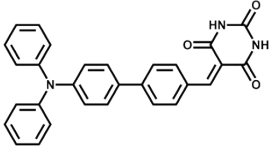
#	Structure		Type		Ref
11		50	Turn on	122	29
12		/	Ratiometric	75	30
13		>3600 and <1800	Turn on	210 110	31
14			Ratiometric	569	32
15		/	Turn on	55	33
16			Turn on	120	34
17		/	Turn off - Turn on	78	35
18		1080	Ratiometric	500	36
19	**UiO-66-Flu**	**3-4**	**Turn on**	**27.17**	**This work**
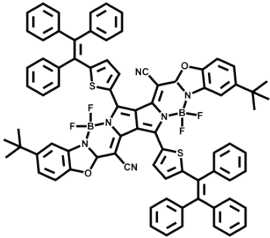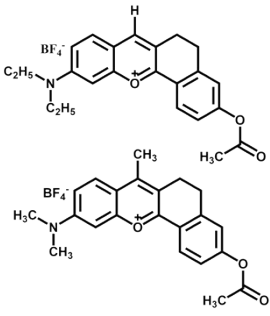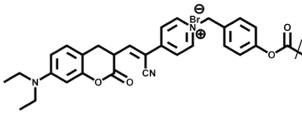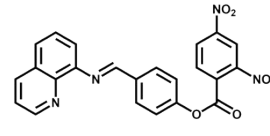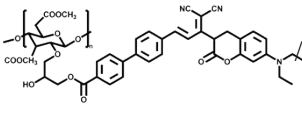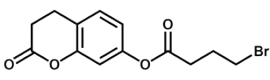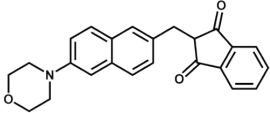
References

1. M. J. Frisch, G. W. Trucks, H. B. Schlegel, G. E. Scuseria, M. A. Robb, J. R. Cheeseman, G. Scalmani, V. Barone, G. A. Petersson, H. Nakatsuji, X. Li, M. Caricato, A. V. Marenich, J. Bloino, B. G. Janesko, R. Gomperts, B. Mennucci, H. P. Hratchian, J. V. Ortiz, A. F. Izmaylov, J. L. Sonnenberg, D. Williams-Young, F. Ding, F. Lipparini, F. Egidi, J. Goings, B. Peng, A. Petrone, T. Henderson, D. Ranasinghe, V. G. Zakrzewski, J. Gao, N. Rega, G. Zheng, W. Liang, M. Hada, M. Ehara, K. Toyota, R. Fukuda, J. Hasegawa, M. Ishida, T. Nakajima, Y. Honda, O. Kitao, H. Nakai, T. Vreven, K. Throssell, J. A. Montgomery, J. E. Peralta, F. Ogliaro, M. J. Bearpark, J. J. Heyd, E. N. Brothers, K. N. Kudin, V. N. Staroverov, T. A. Keith, R. Kobayashi, J. Normand, K. Raghavachari, A. P. Rendell, J. C. Burant, S. S. Iyengar, J. Tomasi, M. Cossi, J. M. Millam, M. Klene, C. Adamo, R. Cammi, J. W. Ochterski, R. L. Martin, K. Morokuma, O. Farkas, J. B. Foresman and D. J. Fox *Gaussian 09, Revision A.02*, Gaussian Inc.: Wallingford, CT, **2016**.
2. F. Weigend, *Phys. Chem. Chem. Phys.*, 2006, **8**, 1057-1065.
3. S. V. Kilina, P. K. Tamukong and D. S. Kilin, *Acc. Chem. Res.*, 2016, **49**, 2127-2135.
4. N. S. Makarov, P. C. Lau, C. Olson, K. A. Velizhanin, K. M. Solntsev, K. Kieu, S. Kilina, S. Tretiak, R. A. Norwood, N. Peyghambarian and J. W. Perry, *ACS Nano*, 2014, **8**, 12572-12586.
5. A. M. Munro, C. Chandler, M. Garling, D. Chai, V. Popovich, L. Lystrom and S. Kilina, *J. Phys. Chem. C.*, 2016, **120**, 29455-29462.
6. S. Kilina, S. Ivanov and S. Tretiak, *J. Am. Chem. Soc.*, 2009, **131**, 7717-7726.
7. L. Lystrom, A. Roberts, N. Dandu and S. Kilina, *Chem. Mater.*, 2021, **33**, 892-901.
8. R. Cammi and J. Tomasi, *J. Comput. Chem.*, 1995, **16**, 1449-1458.
9. F. Weigend and R. Ahlrichs, *Phys. Chem. Chem. Phys.*, 2005, **7**, 3297-3305.
10. T. Lu and Q. Chen, *Comput. Theor. Chem.*, 2021, **1200**, 113249.
11. D. O. Kashinski, G. M. Chase, R. G. Nelson, O. E. Di Nallo, A. N. Scales, D. L. VanderLey and E. F. C. Byrd, *J. Phys. Chem. A.*, 2017, **121**, 2265-2273.
12. C. Lefebvre, G. Rubez, H. Khartabil, J. Boisson, J. Contreras-García and E. Hénon, *Phys. Chem. Chem. Phys.*, 2017, **19**, 17928-17936.
13. S. Kilina, D. Kilin and S. Tretiak, *Chem. Rev.*, 2015, **115**, 5929-5978.
14. M. Kasha, *Discuss. Faraday. Soc.*, 1950, **9**, 14-19.
15. P. Cui, M. Jabed, D. J. Vogel and S. Kilina, *Computational Photocatalysis: Modeling of Photophysics and Photochemistry at Interfaces*, American Chemical Society, 2019, **1331**, 6, 137-156.
16. M. M. Francl, W. J. Pietro, W. J. Hehre, J. S. Binkley, M. S. Gordon, D. J. DeFrees and J. A. Pople, *J. Chem. Phys.*, 1982, **77**, 3654-3665.
17. T. Lu and F. Chen, *J. Comput. Chem.*, 2012, **33**, 580-592.
18. W. Humphrey, A. Dalke and K. Schulten, *J. Mol. Graphics Modell.*, 1996, **14**, 33–38.
19. X. Li, J. Yin, W. Liu, Y. Yang, W. Xu and W. Li, *ChemistrySelect*, 2019, **4**, 14069-14074.
20. N. Vijay and S. Velmathi, *ACS Sustainable Chem. Eng.*, 2020, **8**, 4457-4463.
21. G. Lu, S. Yu, L. Duan, S. Meng, S. Ding and T. Dong, *Luminescence*, 2023, **38**, 1968-1976.

22. Y. Jin, R. Sun, G. Li, M. Yuan, W. Shao, M. Cao, C. Yuan and S. Wang, *Spectrochim. Acta, Part A*, 2023, **294**, 122558.

23. W. Zhang, F. Huo, T. Liu and C. Yin, *J. Mater. Chem. B*, 2018, **6**, 8085-8089.

24. P. Li, Z. Li, X. Miao, H. Hou, M. Wang and X. Yang, *Dalton Trans.*, 2022, **51**, 17787-17794.

25. M. Ruan, B. Zhang, J. Wang, G. Fan, X. Lu, J. Zhang and W. Zhao, *Anal. Methods*, 2023, **15**, 6412-6416.

26. L. Chen, B. Lv, Z. Wang, L. Sun, X. Sun, J. Li and W. Gu, *Dyes Pigm.*, 2023, **220**, 111680.

27. Z. Zhao, L. Xing, Q. Feng and L. Han, *Luminescence*, 2022, **37**, 995-1000.

28. J. Huang, Y. Zhou, W. Wang, J. Zhu, X. Li, M. Fang, Z. Wu, W. Zhu and C. Li, *Spectrochim. Acta, Part A*, 2023, **286**, 122011.

29. A. Karak, M. Mandal, S. Halder, S. Banerjee, D. Banik, A. Maiti, K. Jana and A. K. Mahapatra, *Anal. Methods*, 2022, **14**, 3652-3660.

30. L. Wang, S. Xin, F. Xie, X. Ran, H. Tang and D. Cao, *J. Mater. Chem. C*, 2022, **10**, 14605-14615.

31. Y. Wei, M. Wu, X. Wei, R. Sun, Y. Xu and J. Ge, *Talanta*, 2020, **218**, 121164.

32. P. Liu, W. Wu, Y. Wang, Y. Fan and Z. Xu, *J. Hazard. Mater.*, 2022, **440**, 129713.

33. S. Muthusamy, S. Yin, K. Rajalakshmi, S. Meng, D. Zhu, M. Xie, J. Xie, R. S. Lodi and Y. Xu, *Dyes Pigm.*, 2022, **206**, 110618.

34. J. Kou, Z. Meng, X. Wang, Z. Wang and Y. Yang, *React. Funct. Polym.*, 2023, **182**, 105453.

35. X. Liu, M. Zhu, C. Xu, F. Fan, P. Chen, Y. Wang and D. Li, *Front. Bioeng. Biotechnol.*, 2022, **10**, 937489.

36. H. Su, J. Wang, X. Yue, B. Wang and X. Song, *Spectrochim. Acta, Part A*, 2022, **274**, 121096.